Angular and dynamical properties in resonant inelastic x-ray scattering: Case study of chlorine-containing molecules

Renaud Guillemin, Wayne C. Stolte, Loïc Journel, Stéphane Carniato, Maria Novella Piancastelli, Dennis W. Lindle, and Marc Simon

Phys. Rev. A **86**, 013407 — Published 11 July 2012

DOI: 10.1103/PhysRevA.86.013407

Angular and dynamical properties in resonant inelastic x-ray scattering: case study of chlorine-containing molecules.

Renaud Guillemin,[1] Wayne C. Stolte,[2,3,4] Loïc Journel,[1] Stéphane Carniato,[1]
Maria Novella Piancastelli,[1,*] Dennis W. Lindle,[3] and Marc Simon[1]

[1] *UPMC, Université Paris 06, CNRS, UMR 7614, LCPMR, 11 rue Pierre et Marie Curie, 75231 Paris Cedex 05, France*[†]
[2] *Advanced Light Source, Lawrence Berkeley National Laboratory, Berkeley, California 94720, USA*
[3] *Department of Chemistry, University of Nevada, Las Vegas, Nevada 89154-4009, USA*
[4] *Harry Reid Center for Environmental Studies, University of Nevada, Las Vegas, Nevada, 89154-4003, USA*

(Dated: June 26, 2012)

Polarization-dependent resonant inelastic x-ray scattering (RIXS) has been shown to be a probe of molecular-field effects on the electronic structure of isolated molecules. In this experimental analysis we explain the linear dichroism observed in Cl $2p$ polarized-RIXS following Cl $1s$ excitation of a series of chlorofluoromethanes (CF_3Cl, CF_2Cl_2, $CFCl_3$, and CCl_4) as due to molecular-field effects, including singlet-triplet exchange. We present a novel approach to extract directly the $2p$ inner-shell electronic state populations from the experimental measurements. Using the angular properties of the measured KV emission we also are able to determine the value of the polarization anisotropy parameter β_p for each resolved component of the KV emission spectra.

PACS numbers: 33.80.Eh, 34.50.Gb

I. INTRODUCTION

Dynamics following core excitation in isolated molecules has been extensively studied in recent years, mainly by methods investigating nonradiative decay, i.e., resonant-Auger electron emission, following electron excitation from a core level to an empty molecular orbital or Rydberg state. With such techniques, a wealth of information can be obtained on ultrafast nuclear motion [1–6], ultrafast dissociation processes [7–15], interference phenomena [14], etc. The competing process, i.e. radiative decay, has been less investigated for several reasons. One difficulty is that fluorescence emission is a weak channel for the decay of core-excited states of light elements, where nonradiative decay is dominant. Another reason is that the overall experimental resolution available has until recently made it more advantageous to study electron-kinetic-energy distribution spectra rather than photon-energy distribution spectra.

The main experimental technique to study radiative decay is RIXS (Resonant Inelastic X-ray Scattering). The physical process consists of resonant excitation, in which an inner-shell electron is promoted to an unoccupied orbital, leaving a hole in the core shell, which then relaxes via x-ray photon emission. An inner-shell excitation below the ionization threshold results in x-ray emission spectra sensitive to the energy and bandwidth of the incident radiation. The absorption and emission processes cannot be treated separately and are described by a single transition amplitude, hence the label as a scattering event. Although the ultimate resolution cannot beat that available with electron spectroscopy, RIXS at third-generation synchrotron-radiation facilities has contributed to the understanding of electronic structure and dynamics of isolated atoms and molecules. Furthermore, a new generation of spectrometers is now providing RIXS spectra with vibrational resolution in selected cases [16]. The main advantages of RIXS over resonant-Auger studies are the strict dipole selection rules which govern the excitation-deexcitation processes in most cases and the possibility of exploiting polarization of the x-ray emission. As an example, a dynamical symmetry breaking in molecules occurring on the time scale of the core-hole lifetime was observed due to the symmetry dependence of the x-ray-emission intensities on the selection rules [17, 18]. Polarization and anisotropy of x-ray emission can shed light on orbital components, bond directions, and molecular-orbital symmetries [19–21, 23–25]. Molecular-field effects on the electronic structure of isolated molecules have been observed in the polarization dependence [26, 27], double-ionization cross section [29, 30], and electronic-state interferences [31].

While RIXS is hindered by relatively lower resolution and spectral intensity in the soft x-ray regime compared to resonant-Auger spectroscopy, it has recently been shown to provide very detailed dynamical information in the 2-10 keV photon energy range, including the $1s$ thresholds of Ar, Cl, and $2p$ threshold of I [32–35]. As reported by Simon

*Permanent address: Department of Physics and Astronomy, Uppsala University, PO Box 516, SE-751 20 Uppsala, Sweden
†E-mail: renaud.guillemin@upmc.fr

et al. [33] and Carniato et al. [34] measurements of KL lines using RIXS take advantage of the ultrafast dynamics and high-energy-resolution decay spectra with long-pulse light sources using the concept of effective duration time of the scattering process [36, 37]. In this case, dynamical broadening caused by the Franck-Condon distribution is quenched on top of the photoabsorption resonance, where the width of the KL line approaches the core-hole-lifetime width. Nonlinear dispersion and a significant narrowing of inelastic emission lines around the resonant excitation has also been shown to reflect molecular-bond elongation [33].

Another important feature of RIXS is that anisotropy of polarized x-ray emission from core-excited molecules is well established [19, 20]. Because dipole selection rules impose symmetry restrictions in both absorption and emission [24], and radiative relaxation happens on a short time scale (lifetime $\sim$ 1 fs), excited-state asymmetry is preserved in the decay process because the molecules do not have time to rotate. In our experimental setup, it is possible to vary the angle between the polarization vectors of incident and emitted photons, and therefore to look at the angular properties of KV and KL emission. In particular, linear dichroism observed in Cl $2p$ RIXS following Cl $1s$ excitation in HCl and CF_3Cl [26, 27], and CH_3Cl [28] has been interpreted as a consequence of molecular-field effects, including singlet-triplet exchange, indicating that polarized RIXS provides a direct probe of spin-orbit-state populations applicable to any molecule. In the present work we report an extended comparison between spectroscopic and dynamic properties of the radiative decay in a series of chlorine-containing molecules, namely CCl_4, $CFCl_3$, CF_2Cl_2, and CF_3Cl. From the angular properties of KL and KV emission, we define experimental observables to characterize the polarization anisotropy. Furthermore, we present a novel method to derive spin-orbit-state population from polarization-dependent measurements which can be extracted with a simplified procedure without the need of full theoretical calculations. In the KL decay, we show that the narrowing effect and the nonlinear dispersion of the spectral features across the lowest-lying resonance (excitation to the lowest unoccupied molecular orbital, LUMO) is a common feature along the series of molecules under investigation, because the potential curves of the Cl $1s^{-1}LUMO^*$ and Cl $2p^{-1}LUMO^*$ core-excited states are parallel or nearly so. We confirm that this is a general effect in RIXS and not limited to special cases. In contrast, the spin-orbit-state populations obtained by polarization analysis are different along the series.

II. EXPERIMENTAL SETUP

The measurements were performed at beamline 9.3.1 at the Advanced Light Source, Berkeley CA, which has been previously described elsewhere [38, 39]. In short, beamline 9.3.1 utilizes a double Si(111) monochromator which provides intense (10^{11} photons/sec), monochromatic (0.4 eV at the Cl K edge) and over 99% linearly polarized photons. X-ray emission spectra were acquired using a variable-radius curved-crystal spectrometer consisting of a Si(111) crystal of 2d = 6.271 Å [40] and a thermoelectrically-cooled large-area CCD camera (-74°, 2048×2048 pixels, 27.6×27.6 mm) that can collect an entire spectrum (40 eV wide with 0.5 eV resolution at the Cl K edge) at once. A schematic of the apparatus is shown in Fig. 1. The CF_3Cl, CF_2Cl_2, and $CFCl_3$ samples were maintained at a static pressure of typically 400 Torr, while CCl_4 was held at its room-temperature vapor pressure of 120 Torr. The samples were contained in a $38 \times 38 \times 15$ mm^3 block cell with a 45° angled 3-mm-diameter clearance hole closed on both ends by 2mm×2mm×200μm^3 silicon nitride (Si_3N_4) windows. Samples were obtained commercially, Sigma Aldrich, with stated purities of 99% or greater. The gas cell is positioned in the interior of the Rowland circle, allowing imaging of dispersed gas-phase sample. During data acquisition, the gas cell is tilted at 50° relative to the incoming photon beam. The upstream window serves both as entrance for the incoming photon beam and exit window for the emitted x-rays. Thus, the useful length of the source volume seen by the spectrometer crystal is less than 1 mm which significantly improves the energy resolution of the spectrometer. Because most of the absorption and emission occurs within the first millimeter of the gas sample, self-absorption is minimized and the counting rate is preserved (~ 100 s^{-1} for KV emission). A second Si_3N_4 window is placed at the rear of the gas cell, and unabsorbed x-ray flux transmitted through the gas sample is measured using a Si photodiode for relative absorption measurements.

Energy calibrations of the x-ray-emission spectra were obtained using the positions of previously measured x-ray features [20] and x-rays elastically scattered from the sample. A polynomial equation is fit to the scattered light at up to 25 photon energies across the range of the KL and KV emission to calibrate the energy dispersion of the spectrometer.

The entire apparatus is rotatable around the horizontal axis of the photon beam, and the spectrometer is rotatable around the vertical axis. The latter rotation allows measurements sensitive to the polarization of the emitted photons, as described in previous studies [20, 21, 26–28]. The linear polarization of the photon beam delivered by the beamline is horizontal. The experimental measurements were done with the axis of the spectrometer set vertically, i.e. with $\theta = \pi/2$, where θ is the angle between the emission direction and the incident polarization vector, to allow measurements of the polarization dependencies as a function of χ the angle between the polarization vector of the incoming radiation $\mathbf{e_1}$ and the polarization vector of the emitted radiation $\mathbf{e_2}$ [21].

Finally, the instrument is designed to accurately monitor both the incoming photon flux and sample pressure

continuously during measurements for proper normalization of each spectrum. Particular attention is paid to align the gas cell with the Si(111) crystal along the vertical axis of the spectrometer in order to prevent transmission variation when the spectrometer is rotated as a function of χ. Constant transmission was checked by measuring the KL fluorescence far above threshold where no polarization effect is expected [20].

III. RESULTS

Figures 2 and 3 show the KV and KL radiative decays measured in CCl_4 after Cl $1s$ core excitation as a function of excitation energy around the transition to the LUMO, at $\chi = 0°$ and 90°, respectively. The assignment for KV emission was already reported in [41, 42], albeit with lesser resolution, therefore we suggest an analogous one (see Figs 2 and 3 for details). Chlorofluoromethanes $CFCl_3$, CF_2Cl_2, and CF_3Cl were measured in the same conditions. Figure 4 shows the absorption and KV emission spectra for all four molecules. The related spectral assignments for both absorption and emission are summarized in Table I.

A. Angular properties of KV emission after core excitation

Resonant photoabsorption processes leading to discrete unoccupied molecular orbitals are intrinsically anisotropic because the photoexcited states have definite symmetries, and this anisotropy may be reflected in the angular distribution of the decay processes, such as electron ejection, fluorescence, and photodissociation. A formulation of the polarization properties of fluorescence from atoms and molecules was developed by Fano and Macek [43], and later by Greene and Zare [44] and Luo, Ågren, and Gel'mukhanov [45] using a two-step model to describe the excitation and the subsequent radiative decay. In the latter description, the anisotropy resulting from the symmetries of the electronic states is represented by an alignment parameter A_0 and a geometrical factor $h^{(2)}(J_i, J_f)$ that depends only on the angular-momentum quantum numbers of the initial (J_i) and final (J_f) states (see [44] for more details). Following this formulation, the radiation pattern is fully characterized by the angular distributions and polarizations of the emitted radiation and the emission intensity can be written as a function of the polar coordinates of the x-ray detector (θ) and the angle χ between the incoming and the outgoing polarization vectors:

$$I(\theta, \chi) = \frac{1}{3} I_0 \{1 - \frac{1}{2} h^{(2)}(J_i, J_f) A_0 [P_2(\cos\theta) - \frac{3}{2} \sin^2\theta \cos 2\chi]\}, \quad (1)$$

where I_0 is the total emission intensity and P_2 the second-order Legendre polynomial. All the information that can be obtained by polarization-sensitive measurements of x-ray emission is contained in the term $h^{(2)}(J_i, J_f)A_0$. By analogy with the anisotropy parameter β defined by Cooper and Zare [46] to measure electron or fragment ion anisotropy, we define the polarization anisotropy parameter β_p for photon emission:

$$\beta_p = h^{(2)}(J_i, J_f) A_0. \quad (2)$$

This parameter is related to the anisotropy parameter R defined by Guest *et al.* [47], with $\beta_p = 2R$. For measurements at $\theta = \pi/2$, a typical geometry for synchrotron radiation experiments, Eq. 1 becomes similar to the Cooper-Zare formula for the angular distribution of electrons from a randomly oriented target ionized by 100% linearly polarized light:

$$I(\frac{\pi}{2}, \chi) = \frac{1}{3} I_0 [1 + \frac{\beta_p}{2} (3\cos^2\chi - 1)]. \quad (3)$$

Like the photoelectron asymmetry parameter, β_p is limited to values between -1 and 2. Similarly to the electron angular distributions measured with partially polarized light [48, 49], Eq. 3 can be corrected to account for an imperfect polarimeter, as a function of P, the degree of linear polarization of the emitted photon after diffraction:

$$I(\frac{\pi}{2}, \chi, P) = \frac{1}{3} I_0 [1 + \frac{\beta_p}{4} - \frac{3P\beta_p}{4} + \frac{3P\beta_p}{2} \cos^2\chi]. \quad (4)$$

However, for Si(111) the Bragg reflection condition is fulfilled for 2820 eV at $\theta_B = 44.5°$, close to the x-ray Brewster angle of 45°. As a consequence, the degree of linear polarization P after diffraction is

$$P = \frac{1 - \cos^2(2\theta_B)}{1 + \cos^2(2\theta_B)} = 0.9994, \tag{5}$$

making a Si(111) spectrometer a near-perfect polarimeter for KL emission. Thus, Eq. 3 rather than Eq. 4 can be used to describe the polarization anisotropy measured in the KV emission spectra in this study. The angular properties of KV emission for the chlorofluoromethanes have been discussed in earlier publications [20–22]. These early results were limited to measurements at $\chi = 0°$ and $\chi = 90°$, but demonstrated the usefulness of x-ray polarimetry. In the present study, measurement of the polarization anisotropy parameter β_p as provides an improved probe of molecular-orbital symmetries. In the case of the chlorofluoromethanes, we are able to determine β_p for each resolved component of the KV emission spectra, using Eq. 3 to fit the normalized intensities of each line measured as a function of polarization angle χ for ten angles between 0 and 90° as illustrated in Fig. 5. The values obtained are summarized in Table II. However, a detailed analysis is complicated by the overlap of orbitals with different symmetries, and theoretical calculations are needed to provide a more complete description than the qualitative findings previously reported [20]. In CCl_4, peaks A, B, and C are resolved, and a single value of β_p is given for these three peaks combined, as well as for peaks A and B in $CFCl_3$. We also note that for the elastic peak, X, interferences between resonant and Thomson scattering should be included [50], and the measurement of the polarization anisotropy can be regarded as a measurement of the strength of these interferences. We will address the question of resonant and Thomson scattering interferences in a future publication [51].

B. Dynamical properties of KL emission after core excitation

We have reported in previous studies the dynamical properties of RIXS in chlorine-containing molecules [28, 31, 33–35]. For example, we have shown both experimentally and theoretically, that RXS produces spectral lines without vibrational broadening. This is because both conditions for vibrational collapse (parallelism of the ground and final states, or of the core-excited and final states) are naturally fulfilled in resonant x-ray-Raman scattering, in contrast to resonant-Auger electron scattering. This narrowing of RXS bands is thus predicted to be a general phenomenon. The short lifetime of the core-excited state in the hard-x-ray region leads to a complete breakdown of the conventional nondispersive behavior of soft-x-ray transitions between parallel potential surfaces. In Fig. 6 we show the dispersion and the linewidth of the $2p_{3/2}$ component of the KL lines as a function of photon energy in the interval including the Cl $1s \rightarrow$ LUMO transition in all molecules investigated. It is evident that the phenomenon is exactly the same in all four molecules. Contrary to previous studies where the influence of short lifetime and ultrafast nuclear dynamics was clearly evidenced in HCl [33] and CH_3I [35], no significant differences due to the different masses of the atoms surrounding the C–Cl moiety are present. The present observation suggests that the constituent atoms are heavy enough to limit nuclear dynamics and mask differences among molecules, while the dominant dynamical factor is the local parallelism between the potential curves of the excited and final states.

C. Angular properties of KL emission after core excitation

Theoretical analysis shows that for KL decay the spectral and polarization properties of RIXS are guided by the transition matrix element [53]

$$F^{\alpha\beta}_{2p_\gamma val^*} = \sum_c \frac{\langle 2p_\gamma^{-1} val^{*+1}|\mathcal{D}_\alpha|1s^{-1}val^{*+1}\rangle\langle 1s^{-1}val^{*+1}|\mathcal{D}_\beta|o\rangle}{(\omega_1 - \omega_{cf}) + \imath\Gamma_c/2}, \tag{6}$$

where $|o\rangle$ is the initial (ground) state, $2p_\gamma^{-1}$ is the final state with a hole in one of the three $2p_{x,y,z}$ orbitals ($2p_z$ lies along the symmetry axis), γ represents the spin-orbit (SO) sub-levels, α and β represent the x, y, z components of the dipole operator $\mathcal{D}$, and the frequencies (polarization vectors) of the incident and emitted photons are ω_1 ($\mathbf{e}_1$) and ω_2 ($\mathbf{e}_2$), respectively. Γ_c is the lifetime broadening of the $1s^{-1}val^{*+1}$ neutral core-excited state, and $\hbar\omega_{cf}$ is the transition energy between this state and the final state γ. From symmetry considerations, $\langle 1s^{-1}val^{*+1}|\mathcal{D}_\beta|o\rangle$ vanishes for $\beta = x, y$, and, if the final state has a core hole in $2p_z$, the $\langle 2p_z^{-1}val^{*+1}|\mathcal{D}_{x,y}|1s^{-1}val^{*+1}\rangle$ terms vanish. If the final state has a core hole in $2p_{xy}$, only the terms $\langle 2p_{x,y}^{-1}val^{*+1}|\mathcal{D}_{x,y}|1s^{-1}val^{*+1}\rangle$ do not vanish. Consequently, after averaging over all spatial orientations for randomly oriented molecules, the mean-squared amplitude is given by

$$I_{2p_\gamma}(\chi) \equiv \langle |F_{2p_\gamma val^*}|^2 \rangle = 2(1+2cos^2\chi)[F^{zz}_{2p_z val^*} F^{zz*}_{2p_z val^*}]W^z_{\gamma,S} + 4(2-cos^2\chi)[F^{xy}_{2p_x val^*} F^{xy*}_{2p_x val^*}]W^x_{\gamma,S}, \quad (7)$$

where χ is the angle between $\mathbf{e}_1$ and $\mathbf{e}_2$, and $W^z_{\gamma,S}$ and $W^{x,y}_{\gamma,S}$ are the $2p_z^{-1}val^{*+1}$ and $2p_{x,y}^{-1}val^{*+1}$ populations in the $2p_\gamma^{-1}val^{*+1}$ configuration. This formula explicitly includes the polarization dependency of the $2p_{x,y}$ and $2p_z$ components responsible for the angular dependence experimentally observed in the SO ratio as a function of the angle between the incident and emitted polarization vectors. Because the energy splitting between the $2p_z^{-1}$ and $2p_{x,y}^{-1}$ components ($\sim$ 150 meV) is smaller than the natural lifetime broadening ($\sim$ 0.65 eV), these states are not resolved within the two SO components separated by 1.7 eV. In previous studies[26, 27] we were able to extract the $2p_z$ and $2p_{x,y}$ electronic-state populations by measuring the KL emission lines at 10 different χ angles between 0° and 90°. The analysis of the experimental spectra relied upon theoretical calculations. Derivation of the populations was done by fitting the $2p_{1/2}$ and $2p_{3/2}$ SO peaks with two sub-components each, for a total of four per spectrum. Four-component fits were performed simultaneously for the spectra taken at all ten polarization angles. In this method, the profiles (shapes and widths) used to represent the four components were obtained from theory based on the assumption that the potentials of the $1s^{-1}val^{*+1}$ and $2p_\gamma^{-1}val^{*+1}$ states are parallel. Relative intensities and energy positions of the four components were varied in the multi-spectra fits. This method is illustrated in Fig. 7 for the example of $CFCl_3$, where we show the result of the multi-spectra fit which provides the contribution of each subcomponent for different angles.

Here we simplify the approach in order to extract the electronic-state populations directly from experimental measurements. As demonstrated below, there is an unequivocal relationship between a set of populations and an angle-dependent spin-orbit ratio. As a consequence, only the measurement of the spin-orbit ratio as a function of the angle between the incident and emitted polarization vectors is necessary to extract unambiguously the electronic-state populations. Following Eq. 7 we can write the spin-orbit ratio as

$$R_{SO}(\chi) = \frac{I_{2p_{3/2}}(\chi)}{I_{2p_{1/2}}(\chi)} = \frac{2[1+2\cos^2\chi](1-W^z_{1/2}) + 4[2-\cos^2\chi](1-W^x_{1/2})}{2[1+2\cos^2\chi]W^z_{1/2} + 4[2-\cos^2\chi]W^x_{1/2}} \quad (8)$$

where $W^z_{1/2}$ and $W^x_{1/2}$ are the populations in the $2p_z(1/2)$ and $2p_x(1/2)$, respectively, and the transition probabilities between the Cl $1s$ state and the $2p$ components are assumed to be equals for all subcomponents due to the parallelism of the potential-energy curves [27], i.e., $F^{zz}_{2p_z val^*} = F^{xy}_{2p_x val^*}$. This equation can be used to fit the experimental ratios using the populations $W^z_{1/2}$ and $W^x_{1/2}$ as the only parameters.

For Si(111), the Bragg reflection condition is fulfilled for 2620 eV at $\theta_B = 49°$. This deviation from the Brewster angle, 45°, results in a partial polarization after diffraction:

$$P = \frac{1-\cos^2(2\theta_B)}{1+\cos^2(2\theta_B)} = 0.962. \quad (9)$$

To account for this small effect, we need to correct for the amount of unpolarized light transmitted by the polarimeter. For perpendicular-polarized emission, the angle between the incident polarization vector and the emitted polarization vector is 90°, and

$$I_\perp = I_{2p_\gamma}(\pi/2) = 2[F^2]W^z_{\gamma,S} + 8[F^2]W^x_{\gamma,S}.$$

For parallel-polarized emission, the angle between the incident polarization vector and the emitted polarization vector is 0°, and

$$I_\parallel = I_{2p_\gamma}(0) = 6[F^2]W^z_{\gamma,S} + 4[F^2]W^x_{\gamma,S}.$$

The contribution of unpolarized light is the sum of these two contributions [48]:

$$I_{unpol} = I_\parallel + I_\perp = 8[F^2]W^z_{\gamma,S} + 12[F^2]W^x_{\gamma,S}.$$

The total intensity can be written as a function of χ as the weighted sum of contributions from polarized light and unpolarized, with P the degree of linear polarization, as

$$\begin{aligned} I_{2p_\gamma}(\chi,P) &= P\{2(1+2\cos^2\chi)[F^2]W^z_{\gamma,S}+4(2-\cos^2\chi)[F^2]W^x_{\gamma,S}\} \\ &\quad +(1-P)\{8[F^2]W^z_{\gamma,S}+12[F^2]W^x_{\gamma,S}\}. \end{aligned}$$

Finally, we obtain the SO ratio:

$$R_{SO}(\chi,P)=\frac{[4-3P+2P\cos^2\chi](1-W^z_{1/2})+2[3-P-P\cos^2\chi](1-W^x_{1/2})}{[4-3P+2P\cos^2\chi]W^z_{1/2}+2[3-P-P\cos^2\chi]W^x_{1/2}}. \quad (10)$$

Figure 8 shows experimental ratios and fits using Eq. 10 on a variety of chlorine-containing molecules. Electronic-state populations derived from the fits in Fig. 8 are summarized in Table III. The HCl and CF_3Cl data were published previously in [26, 27]. The Cl_2 data come from unpublished results. It is clear from the experimental data and results from the fits that small variations in populations lead to large changes in the observed SO ratios. For instance, the SO ratios measured at 0 and 90 degrees in HCl are 1.19±0.01 and 1.42±0.01, respectively, and the derived populations are $2p_z(1/2)$=50% and $2p_x(1/2)$=39%. By comparison, the SO ratios in CCl_4 are 1.38±0.01 and 1.62±0.01, at 0 and 90 degree, with electronic-states populations of $2p_z(1/2)$=46% and $2p_x(1/2)$=36%. Using Eq. 8, instead of Eq. 10, to fit the experimental SO ratios, would lead to a systematic error of about 1% in the electronic state populations, larger than the ±0.5% experimental error bars. As a consequence, the electronic populations obtained when taking into account the linear degree of polarization in HCl are in better agreement with the calculated values ($2p_z(1/2)$=49% and $2p_x(1/2)$=39.5%) than the experimental values published previously [26, 27]. This demonstrates that by using a simple relationship (Eq. 10), we can experimentally derive a unique set of $2p_{x,y,z}$ electronic-state populations. The good agreement with theoretical calculations for HCl and CF_3Cl validates the experimental method presented in this study. We also note that Eq. 10 can be used to derive experimentally electronic states populations from angle-resolved RIXS measurements for any core-excited molecular systems, at any Bragg angles, i.e., at energies where the spectrometer is an imperfect polarimeter. Obviously, however, partial polarization will result in a loss of sensitivity. The main limit of this method comes from the ability to isolate the KL emission from the $1s^{-1}LUMO^*$ core-excited state. From a general point of view, the excitation of several overlapping states will result in overlapping KL lines. For instance, close-lying Rydberg states may be excited at the energy of the transition to the LUMO, affect the experimental KL spectra, and lead to error in the electronic populations. Among the molecules studied here, we can distinguish two extreme cases. In the case of HCl, the first Rydberg state is well separated from the main resonance in the absorption spectrum (see for instance Fig. 5 in [27]). The determination of the electronic populations is straightforward. In the case of CCl_4, the first Rydberg state overlaps substantially with the main resonance (see transition 2 in Fig. 4), and may affect the determination of the populations. In such a case, theoretical calculations can help to disentangle the KL spectra, as recently shown in the study of interference effects in x-ray emission [31].

IV. CONCLUSION

In conclusion, we have studied a series of chlofluoromethanes, CCl_4, $CFCl_3$, CF_2Cl_2, and CF_3Cl, to deepen our understanding of the angular properties of inelastic x-ray scattering in the gas phase. We show that while the dynamical properties of the KL emission are identical for these molecules, the angular properties of both KV and KL emission show large differences. We also derive a simple method to extract the $2p_{x,y,z}$ electronic-state populations directly from the measurement of polarization-dependent KL spectra. Polarized RIXS is a powerful tool to investigate the chemical properties of isolated molecules.

V. ACKNOWLEDGEMENTS

The authors would like to express their gratitude to the staff of the Advanced Light Source (ALS) for their valuable help. Support from the National Science Foundation under NSF Grant No. PHY-01-40375 is gratefully acknowledged. The Advanced Light Source is supported by DOE (DE-AC03-76SF00098). M.N.P. acknowledges the French Agence Nationale de la Recherche (ANR) for financial support in the framework of "Chair d'Excellence" program.

[1] M. Simon, P. Morin, P. Lablanquie, M.Lavollée, K. Ueda, and N. Kosugi, Chem. Phys. Lett. **238**, 42 (1995).
[2] M. Simon, C. Miron, N. Leclercq, P. Morin, K. Ueda, Y. Sato, S. Tanaka, and Y.Kayanuma, Phys. Rev. Lett. **79**, 3857 (1997).
[3] C. Miron, R. Guillemin, N. Leclerq, P. Morin, and M. Simon, J. Electr. Spectrosc. Relat. Phenom. **93**, 95 (1998).
[4] P. Morin, M. Simon, C. Miron, N. Leclercq, E. Kukk, J.D. Bozek and N. Berrah, Phys.Rev. A **61**, 050701 (2000).
[5] C. Miron, M. Simon, P. Morin, S. Nanbu, N. Kosugi, S.L. Sorensen, A. Naves de Brito, M.N. Piancastelli, O. Björneholm, R. Feifel, M. Bässler, and S. Svensson, J. Chem. Phys. **115**, 86 (2001).
[6] C. Miron, R. Feifel, O. Björneholm, S.Svensson, A. Naves de Brito, S.L. Sorensen, M.N. Piancastelli, M. Simon and P. Morin, Chem. Phys. Lett. **359**, 48 (2002).
[7] P. Morin and I. Nenner, Phys. Rev. Lett. **56**, 1913 (1986).
[8] E. Kukk, H. Aksela, O.-P. Sairanen, S. Aksela, A. Kivimäki, E. Nõmmiste, A. Ausmees, A. Kikas, S.J. Osborne and S. Svensson, J. Chem. Phys. **104**, 4475 (1996).
[9] A. Menzel, B. Langer, J. Viefhaus, S.B. Whitfield, and U. Becker, Chem. Phys. Lett. **258**, 265 (1996).
[10] O. Björneholm, S. Sundin, S. Svensson, R.T. Marinho, A. Naves de Brito, F. Gel'mukhanov, and H. Ågren, Phys. Rev. Lett. **79**, 3150 (1997).
[11] K. Ueda, Y. Muramatsu, H. Chiba, Y. Sato, and E. Shigemasa, J. Electron Spectrosc. Relat. Phenom. **88-91**, 53 (1998).
[12] I. Hjelte, M.N. Piancastelli, R.F. Fink, O. Björneholm, M. Bässler, R. Feifel, A. Giertz, H. Wang, K. Wiesner, A. Ausmees, C. Miron, S.L. Sorensen, and S. Svensson, Chem. Phys. Lett. **334**, 151 (2001).
[13] I. Hjelte, M.N. Piancastelli, C.M. Jansson, K. Wiesner, O. Björneholm, M. Bässler, S.L. Sorensen, and S. Svensson, Chem. Phys. Lett. **370**, 781 (2003).
[14] R. Feifel, F. Burmeister, P. Sałek, M.N. Piancastelli, M. Bässler, S.L. Sorensen, C. Miron, H. Wang, I. Hjelte, O. Björneholm, A. Naves de Brito, F.Kh. Gel'mukhanov, H. Ågren, and S. Svensson, Phys. Rev. Lett. **85**, 3133 (2000).
[15] R.F. Fink, A. Eschner, M. Magnuson, O. Björneholm, I. Hjelte, C. Miron, M. Bässler, S. Svensson, M.N. Piancastelli and S.L. Sorensen, J. Phys. B: At. Mol. Opt. Phys. **39**, L269 (2006).
[16] F. Hennies, A. Pietzsch, M. Berglund, A. Föhlisch, T. Schmitt, V. Strocov, H.O. Karlsson, J. Andersson, and J.-E. Rubensson, Phys. Rev. Lett. **104**, 193002 (2010).
[17] P. Skytt, P. Glans, J.-H. Guo, K. Gunnelin, C.Såthe, J. Nordgren, F. Kh. Gel'mukhanov, A. Cesar, and H. Ågren, Phys. Rev. Lett. **77**, 5035 (1996).
[18] P. Glans, K. Gunnelin, P. Skytt, J.H. Guo, N. Wassdahl, J. Nordgren, H. Ågren, F. Gel'mukhanov, T. Warick, and E. Rotenberg, Phys. Rev. Lett. **76**, 2448 (1996).
[19] D.W. Lindle, P.L. Cowan, R.E. LaVilla, T. Jach, R.D. Deslattes, B. Karlin, J.A.S heehy, T.J. Gil, and P.W.Langhoff, Phys. Rev. Lett. **60**, 1010 (1988).
[20] D.W. Lindle, P.L. Cowan, T. Jach, R.E. LaVilla, and R.D. Deslattes, Phys. Rev. A **43**, 2353 (1991).
[21] S.H. Southworth, D.W. Lindle, R. Mayer, and P.L. Cowan, Phys. Rev. Lett. **67**, 1098 (1991).
[22] S.H. Southworth, D.W. Lindle, R. Mayer, and P.L. Cowan, Nucl. Instrum. Phys. Res. B, **56-57**, 304 (1991).
[23] R.C.C. Perera, P.L. Cowan, D.W. Lindle, R.E. LaVilla, T. Jach, and R.D. Deslattes, Phys. Rev. A **43**, 3609 (1991).
[24] J.D. Mills, J.A. Sheehy, T.A. Ferrett, S.H. Southworth, R. Mayer, D.W. Lindle, and P.W.Langhoff, Phys. Rev. Lett. **79**, 383 (1997).
[25] K.E. Miyano, U. Arp, S.H. Southworth, T.E. Meehan, T.R. Walsh, and F.P. Larkins, Phys. Rev. A **57**, 2430 (1998).
[26] R. Guillemin, S. Carniato, W.C. Stolte, L. Journel, R. Taïeb, D.W. Lindle, and M. Simon, Phys. Rev. Lett. **101**, 133003 (2008).
[27] S. Carniato, R. Guillemin, W.C. Stolte, L. Journel, R. Taïeb, D.W. Lindle, and M. Simon, Phys. Rev. A **80**, 032513 (2009).
[28] L. El Khoury, L. Journel, R. Guillemin, S. Carniato, W.C. Stolte, T. Marin, D.W. Lindle, and M. Simon, J. Chem. Phys. **136**, 024319 (2012).
[29] J. Hoszowska, A.K. Kheifets, J.-Cl. Dousse, M. Berset, I. Bray, W. Cao, K. Fennane, Y. Kayser, M. Kavčič, J. Szlachetko, and M. Szlachetko, Phys. Rev. Lett. **102**, 073006 (2009).
[30] M. Kavčič, M.Žitnik, K.Bučar, A.Mihelič, M.Štuhec, J. Szlachetko, W. Cao, R. Alonso Mori, and P. Glatzel, Phys. Rev. Lett. **102**, 143001 (2009).
[31] M. Kavčič, M. Žitnik, K. Bučar, A. Mihelič, S. Carniato, L. Journel, R. Guillemin, and M. Simon, Phys. Rev. Lett. **105**, 113004 (2010).
[32] P.A. Raboud, M. Berset, J.-Cl. Dousse, Y.-P. Maillard, O. Mauron, J. Hoszowska, M. Polasik, and J. Rzadkiewicz, Phys.Rev. A **65**, 062503 (2002).
[33] M. Simon, L. Journel, R. Guillemin, W. C. Stolte, I. Minkov, F.Gel'mukhanov, P. Sałek, H. Ågren, S. Carniato, R. Taïeb, A. C. Hudson, and D. W. Lindle, Phys. Rev. A **73**, 020706 (2006).
[34] S. Carniato, R. Taïeb, R. Guillemin, L. Journel, M. Simon, F. Gel'mukhanov, Chem. Phys. Lett **439**, 402 (2007).
[35] T. Marchenko, L. Journel, T. Marin, R. Guillemin, S. Carniato, M. Žitnik, M. Kavčič, K. Bučar, A. Mihelič, W. Cao, and M. Simon, J. Chem. Phys. **134**, 144308 (2011).
[36] F. Gel'mukhanov, P. Sałek, T. Privalov, and H. Ågren, Phys. Rev. A **59**, 380 (1999).
[37] F. Gel'mukhanov and H. Ågren, Phys. Rep. **312**, 87 (1999).
[38] R.C.C. Perera, G. Jones, and D.W. Lindle, Rev. Sci. Instrum. **66**, 1745 (1995)
[39] G. Jones, S. Ryce, D.W. Lindle, B.A. Karlin, J.C. Woicik, and R.C.C. Perera, Rev. Sci. Instrum. **66**, 1748 (1995)

[40] A.C. Hudson, W.C. Stolte, R. Guillemin, and D.W. Lindle, Rev. Sci. Instrum. **78**, 053101 (2007).
[41] R.C.C. Perera and B.L. Henke, J. Chem. Phys. **70**, 5398 (1979).
[42] R.C.C. Perera, R.E. LaVilla, and G.V. Gibbs, J. Chem. Phys. **86**, 4824 (1987).
[43] U. Fano and J.H. Macek, Rev. Mod. Phys. **45**, 553 (1973).
[44] C.H. Greene and R.N. Zare, Ann. Rev. Phys. Chem. **33**, 119 (1982).
[45] Yi Yuo, H Ågren, and F. Gel'mukhanov, Phys. Rev. A **53**, 1340 (1996).
[46] J. Cooper and R.N. Zare, J. Chem. Phys. **48**; 942 (1968).
[47] J.A. Guest, K.H. Jackson, and R.N. Zare, Phys. Rev. A **28**, 2217 (1983).
[48] J.A.R. Samson and A.F. Starace, J. Phys. B: Atom. Mol. Phys. **8**, 1806 (1975).
[49] P.S. Shaw, U. Arp, and S.H. Southworth, Phys. Rev. A **54**, 1463 (1996).
[50] V.A. Yavna, A.N. Hopersky, A.M. Nadolinsky and S.A. Yavna, J. Phys. B: Atom. Mol. Phys. **33**, 3249 (2000).
[51] S. Carniato *et al.*, to be published.
[52] W. Zhang, T. Ibuki, and C.E. Brion, Chem. Phys. **160**, 435 (1992).
[53] J.J. Sakurai, In *Advanced Quantum Mechanics*. Addison-Wesley (1967).

TABLE I: Assignments from [23, 42, 52]

	CCl_4	$CFCl_3$	CF_2Cl_2	CF_3Cl
			Absorption	
1	$(7a_1)$	$(12a_1)$	$(13a_1 + 9b_2)$	$(11a_1)$
2	$(8t_2)$	$(11e + 13a_1)$	$(14a_1 + 7b_1)$	$(12a_1 + 8e)$
3	$4p$	$4p$	$4p$	$4p$
			Emission	
X	elastic	elastic	elastic	elastic
A	$(2t_1)$	$(2a_2 + 10e)$	$(8b_2)$	$(7e)$
B	$(7t_2)$	$(9e + 11a_1)$	$(6b_1 + 3a_2)$	$(10a_1)$
C	$(2e)$	$(8e)$	$(5b_1 + 7b_2 + 12a_1)$	$(5e)$
D	$(6t_2)$	$(7e)$	$(11a_1 + 4b_1)$	$(9a_1 + 4e)$

TABLE II: Experimental anisotropy parameters β_p for individual or groups of emission lines in chlorine-containing molecules. Assignments are given in Table I.

	CCl_4	$CFCl_3$	CF_2Cl_2	CF_3Cl
X	1.44±0.03	1.42±0.05	1.48±0.05	1.65±0.14
A	-0.66±0.03	-0.47±0.02	-0.49±0.02	-0.55±0.02
B	–	–	0.27±0.03	0.44±0.03
C	–	0.1±0.06	0.20±0.05	1.05±0.28
D	0.1±0.07	0.43±0.08	0.46±0.08	0.51±0.13

TABLE III: Experimental $2p_z$ and $2p_{x,y}$ electronic-states populations ($\pm 0.5\%$) derived from the angle-dependent spin-orbit ratios for a variety of chlorine-containing molecules.

	$2p_z(1/2)$	$2p_{x,y}(1/2)$	$2p_z(3/2)$	$2p_{x,y}(3/2)$
HCl	50%	39%	50%	61%
Cl_2	54%	34%	46%	66%
CCl_4	46%	36%	54%	64%
$CFCl_3$	48.5%	35%	51.5%	65%
CF_2Cl_2	50%	35%	50%	65%
CF_3Cl	53.5%	40%	46.5%	60%

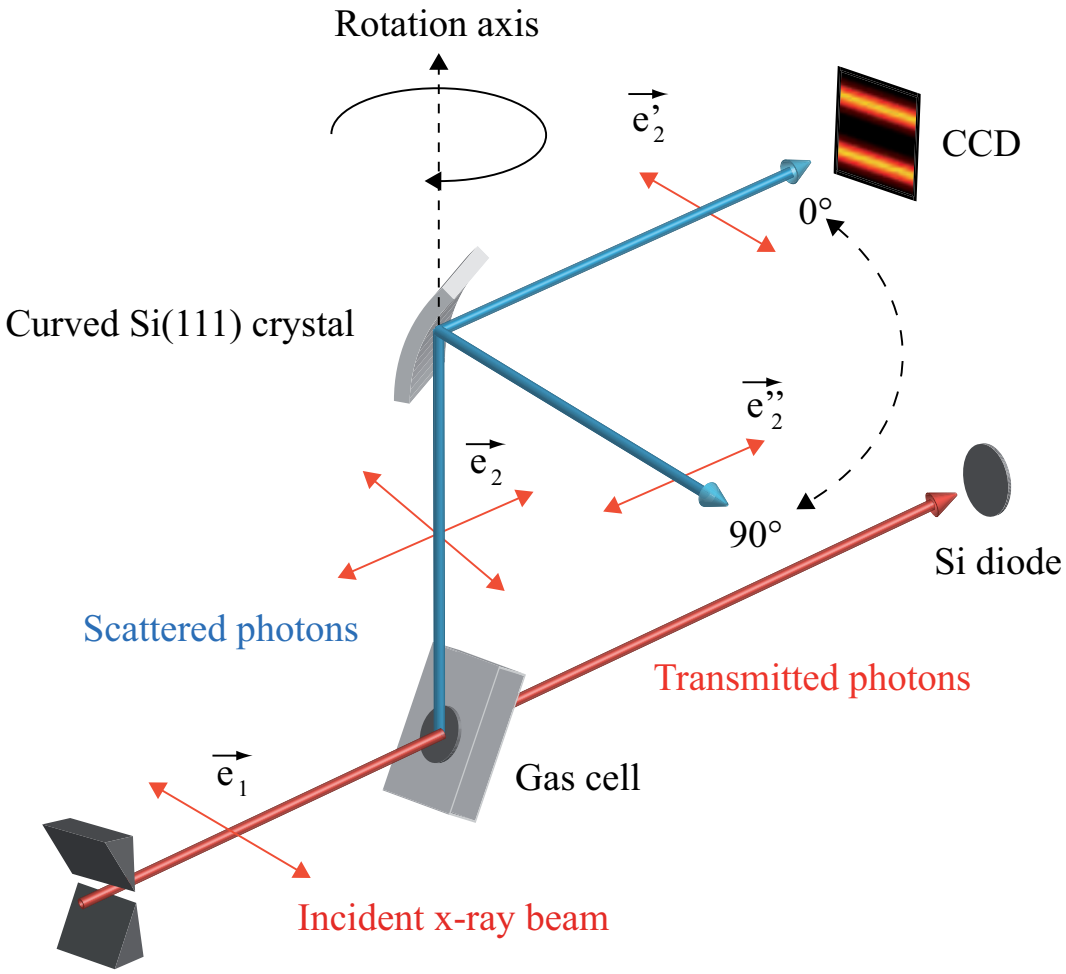

FIG. 1: (Colors online) Schematic of the polarized-x-ray spectrometer used at the ALS.

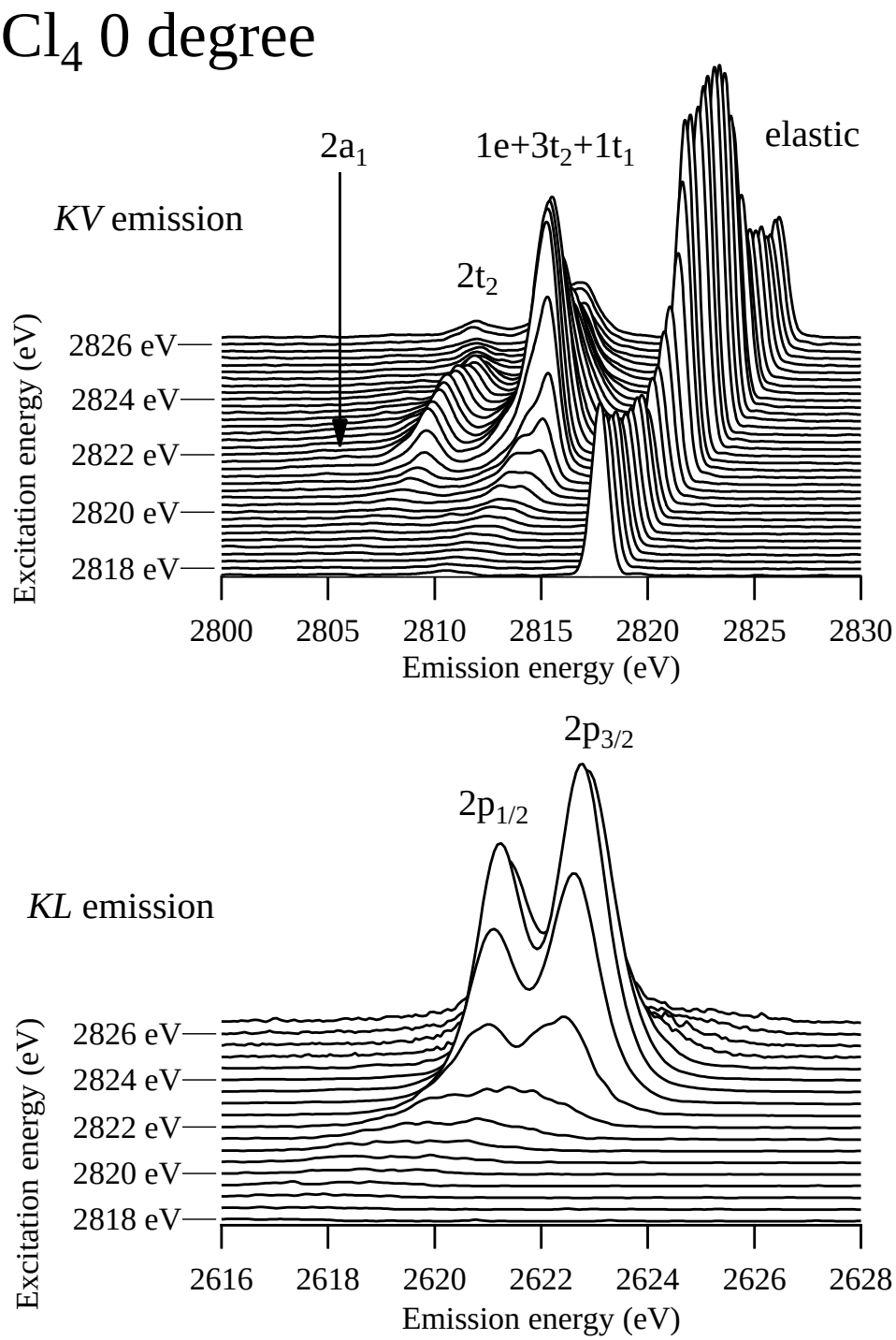

FIG. 2: KV and KL emission spectra from CCl_4 recorded at photon energies around the Cl1$s \rightarrow 7a_1$ resonance ($h\nu = 2822.5$ eV) at 0° with respect to the incident polarization.

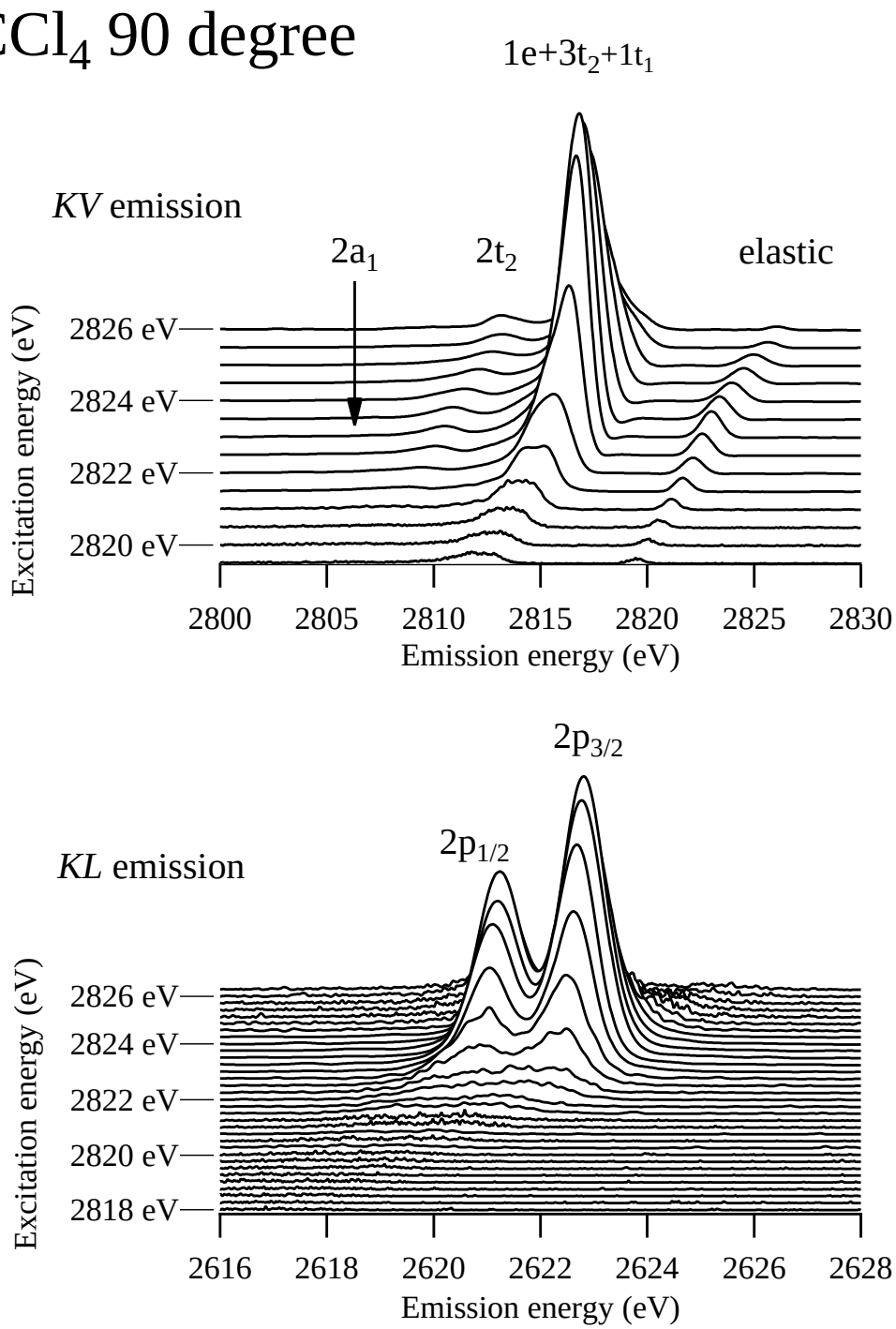

FIG. 3: KV and KL emission spectra from CCl_4 recorded at photon energies around the Cl1$s \rightarrow 7a_1$ resonance ($h\nu = 2822.5$ eV) at 90° with respect to the incident polarization.

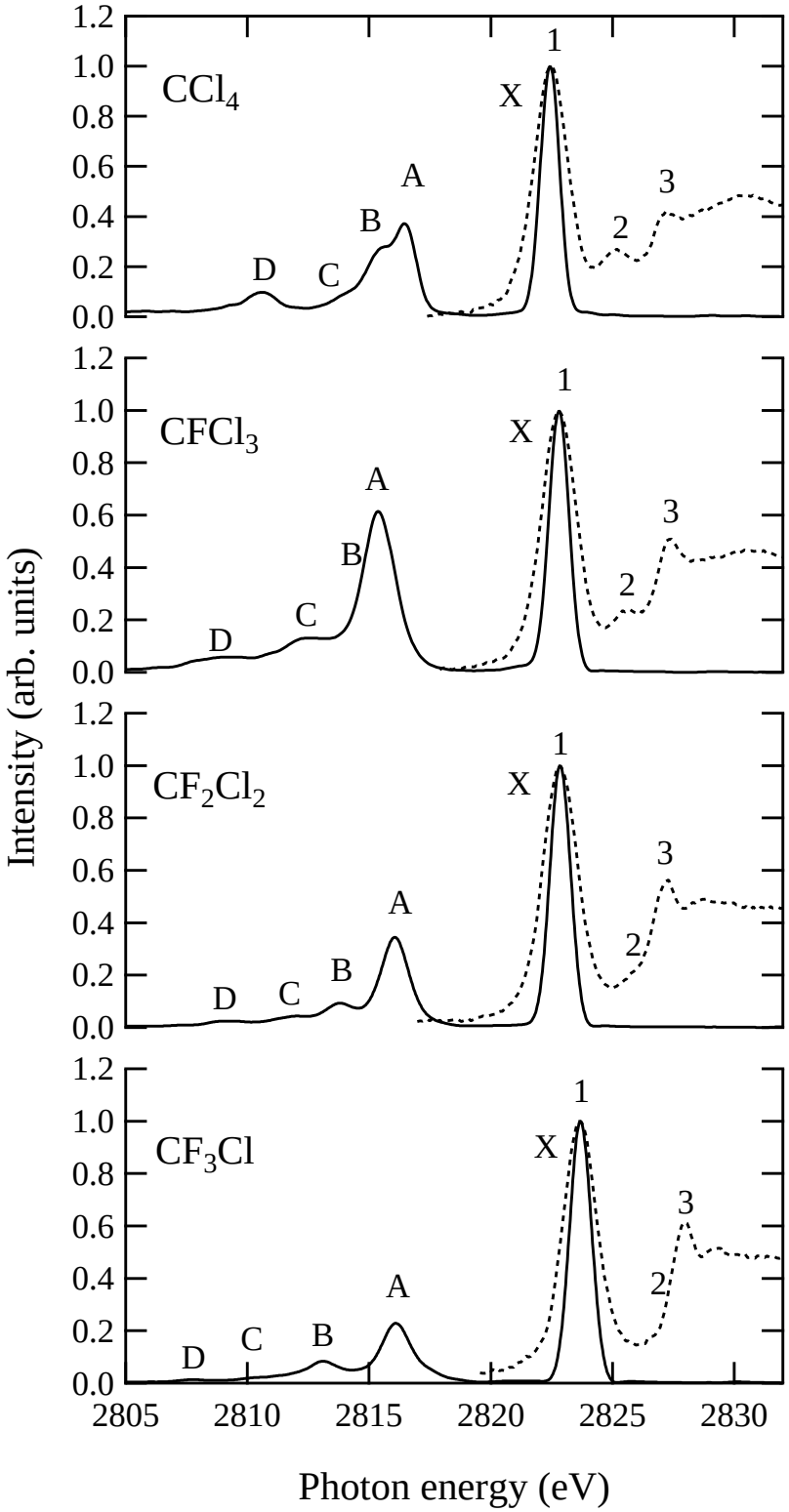

FIG. 4: Absorption (dashed) and KV emission spectra (solid) for CCl_4, $CFCl_3$, CF_2Cl_2, and CF_3Cl. Emission spectra are recorded at the maximum of the Cl1$s \rightarrow LUMO$ resonances. Labels refer to assignments given in Table I.

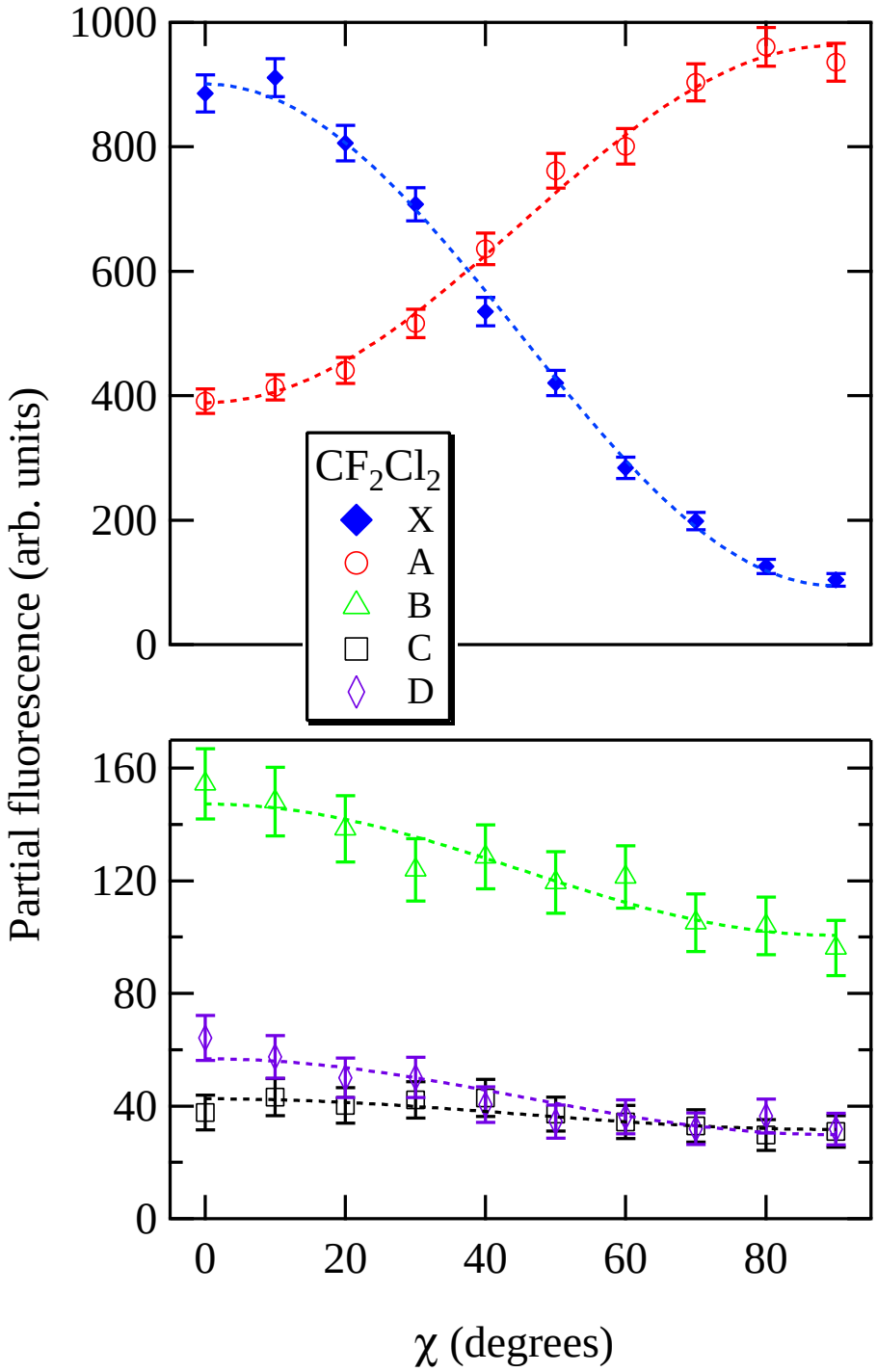

FIG. 5: (Colors online) Angular dependence of the KV emission lines from CF_2Cl_2 as a function of polarization angle χ. Labels refer to assignments in Table I

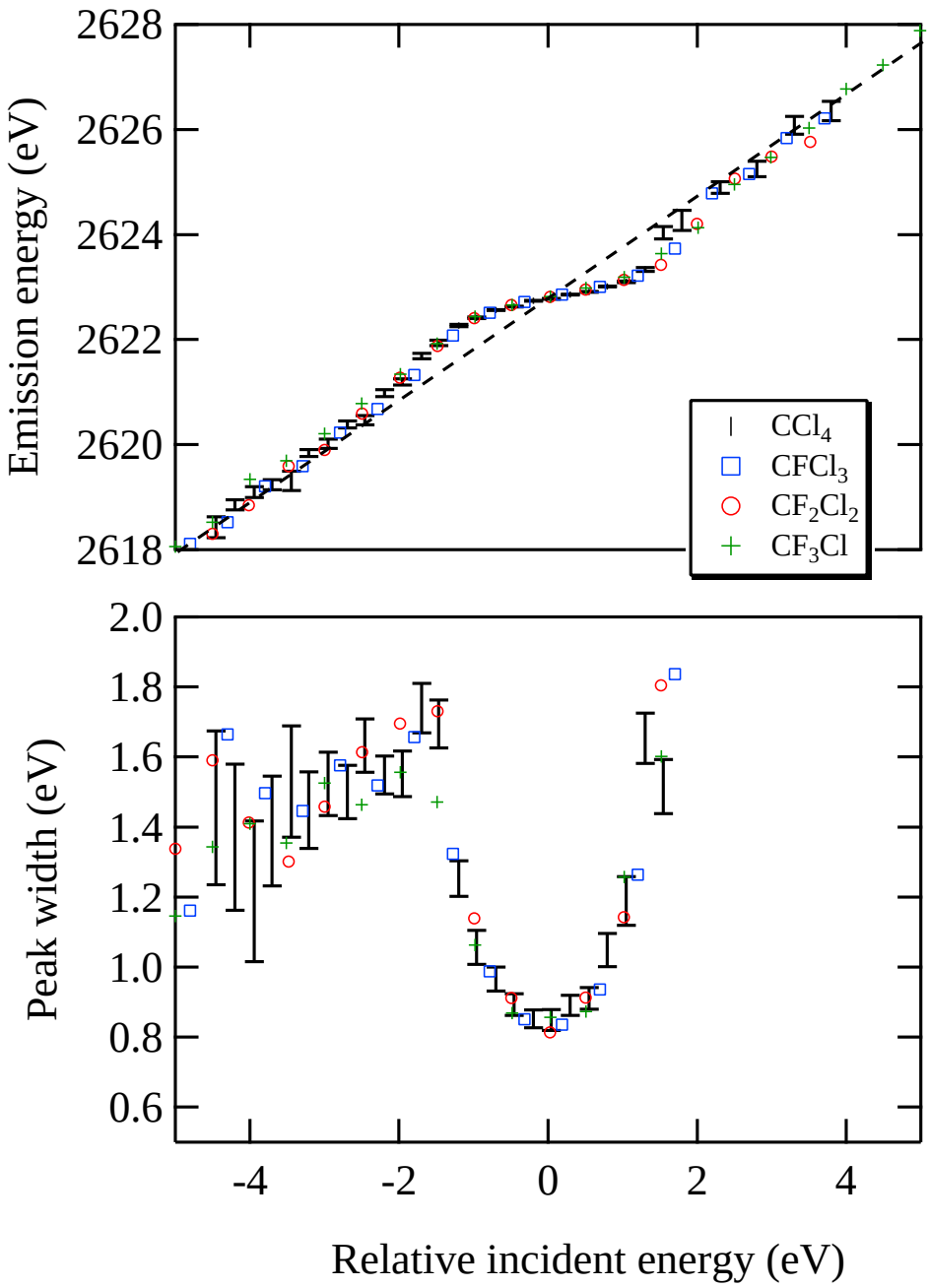

FIG. 6: (Colors online) Dispersion (top) and width (bottom) of the $2p_{3/2}$ spin-orbit component in KL emission from CCl_4, $CFCl_3$, CF_2Cl_2, and CF_3Cl, as a function of energy detuning with respect to the Cl1$s \rightarrow LUMO$ resonances. Experimental values were obtained at $\chi = 90°$. No differences were observed for other angles. For clarity errors bars are given only for CCl_4 and reflect the errors bars obtained for all other molecules presented in the figure.

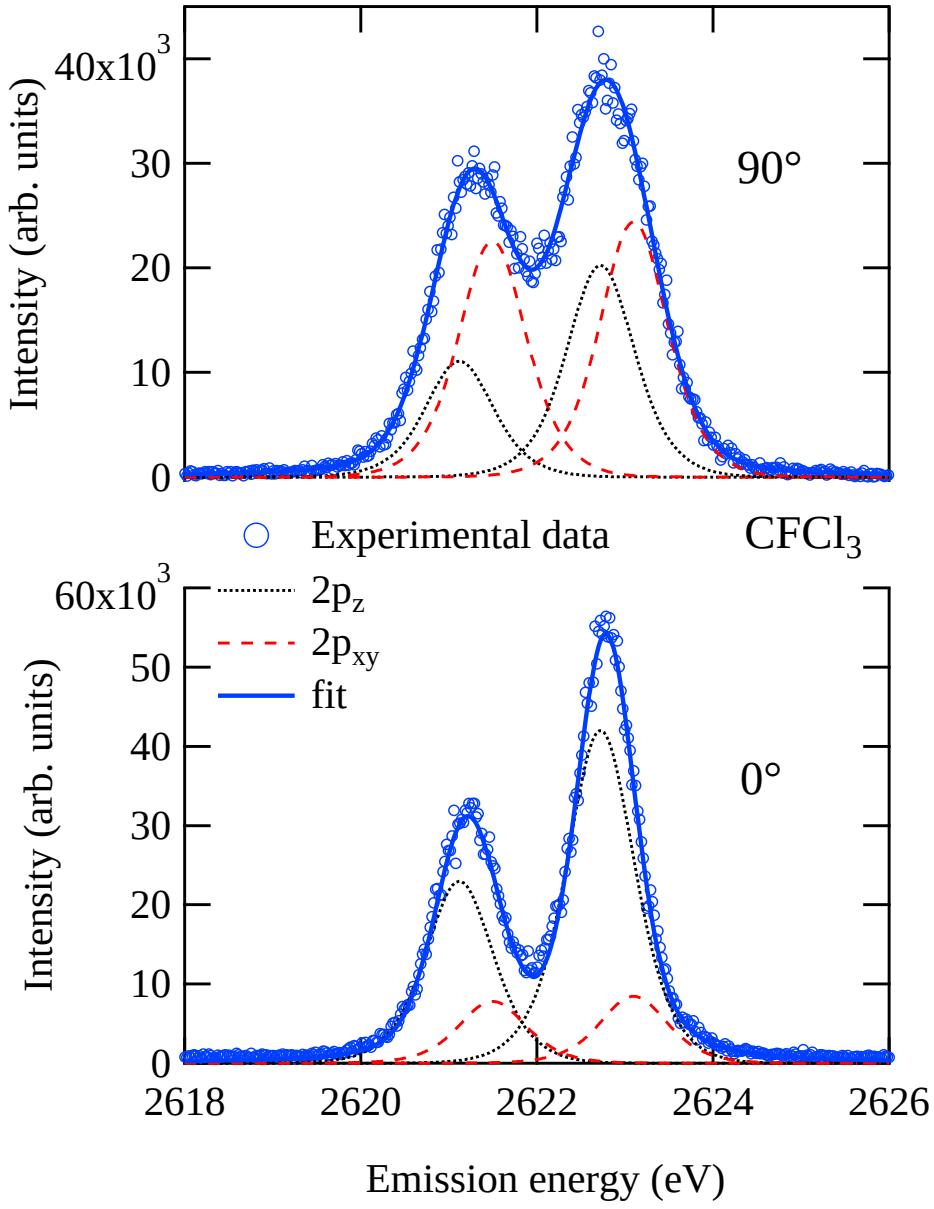

FIG. 7: (Colors online) $2p_z$ and $2p_{x,y}$ subcomponents of the spin-orbit doublet in KL emission from $CFCl_3$ as a function of polarization angle. Incident photon energy was set at the maximum of the $Cl1s \rightarrow 12a_1$ resonance.

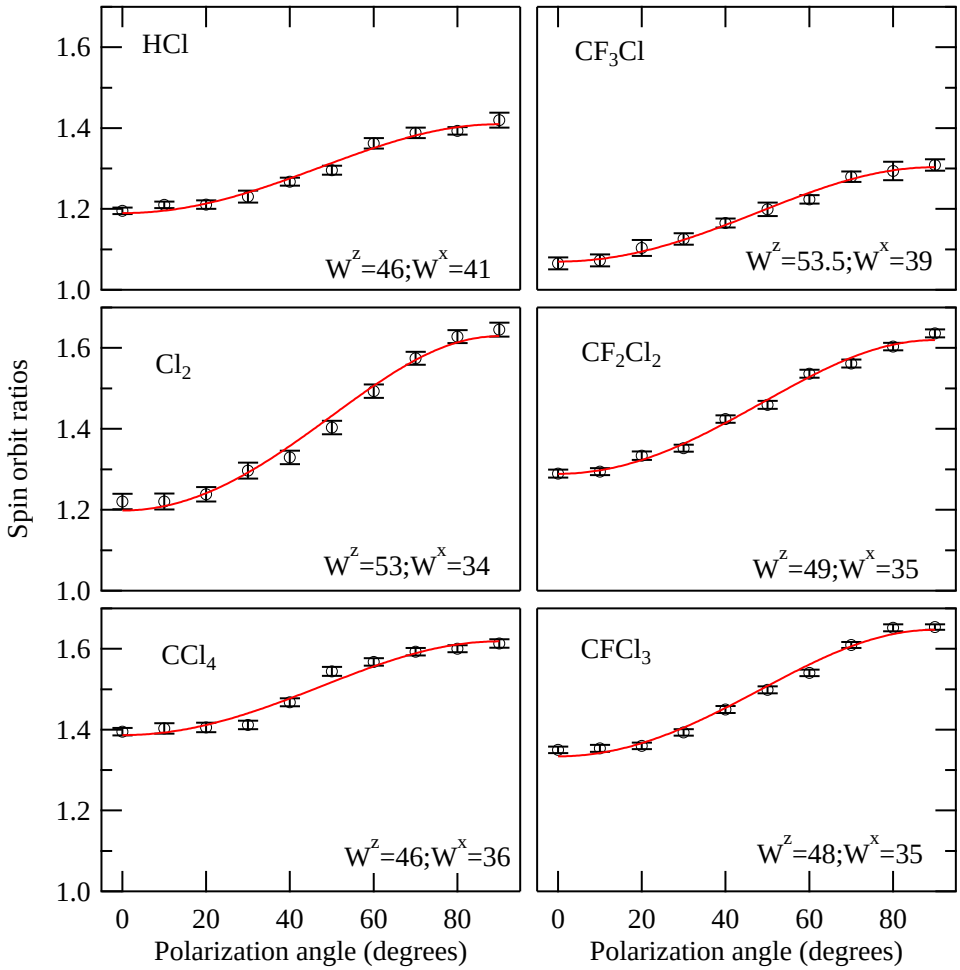

FIG. 8: (Colors online) Spin-orbit ratios and electronic-state populations for various molecules measured as a function of polarization angle χ. Circles are experimental data, and solid lines are fits using Eq. 10. Electronic-state populations are given in Table III.